Non-equilibrium theory of charge qubit decoherence in the quantum point contact measurement

Ming-Tsung Lee[a] **and Wei-Min Zhang**[a,b]
[a] *National Center for Theoretical Science, Tainan, Taiwan 70101, R.O.C.*
[b] *Department of Physics and Center for Quantum Information Science, National Cheng Kung University, Tainan, Taiwan 70101, R.O.C.*
(Dated: April 19, 2008)

A non-equilibrium theory describing the charge qubit dynamics measured by a quantum point contact is developed based on Schwinger-Keldysh's approach. Using the real-time diagram technique, we derive the master equation to all orders in perturbation expansions. The non-Markovian processes in the qubit dynamics is naturally taken into account. The qubit decoherence, in particular, the influence of the tunneling-electron fluctuation in the quantum point contact with a longer time correlation, is studied in the framework. We consider the Lorentzian-type spectral density to characterize the channel mixture of the electron tunneling processes induced by the measurement and determine the correlation time scale of the tunneling-electron fluctuation. The result shows that as the quantum point contact is casted with a narrower profile of the spectral density, tunneling electrons can propagate with a longer time correlation and lead to the non-Markovian processes of the qubit dynamics. The qubit electron in the charge qubit will be driven coherently. The quantum point contact measurement with the minimum deviation of the electron tunneling processes prevents the qubit state from the decoherence.

PACS numbers: 03.65.Yz,73.23.-b,05.70.Ln,03.67.Lx

I. INTRODUCTION

With the rapid progress in nano-technology, the investigation of quantum processes in systems coupling to a mesoscopical measurement device becomes a very active research field in recent years.[1, 2, 3, 4] Not only its practical application to quantum communication and quantum computation,[5] but also the theoretical interests in the measurement-induced quantum decoherence [3, 6] have attracted much attention. In particular, in the investigation of the solid-state quantum computer with charge qubits, the quantum point contact (QPC) has been served as an ultrasensitive electrometer [1, 7, 8, 9, 10]. In the literature, the measurement of charge qubit through the QPC has been treated based on the so-called Markovian approximation,[11, 12, 13, 14] in which the time scale of the qubit dynamics is assumed much larger than that of the tunneling-electron correlation in the QPC. This theoretical treatment based on the Markovian approximation describes only the qubit dynamics in the time-asymptotic quasi-equilibrium state. Mesoscopically, the qubit decoherence occurs in the time scale of the same order of the tunneling-electron correlation time in the QPC, where the non-Markovian dynamics of the qubit is significant. Thus, a non-equilibrium description to the qubit dynamics is more desired. Recently, the considerations of the solid-state system processing in the non-Markovian regime have indeed received more attention. For instance, a local electron spin coupling with a nuclear spin bath through the Fermi contact hyperfine interaction in which the electron spin dynamics is in the time scale shorter than the nuclear dipole-dipole correlation time[15], and electron transports of interacting electron systems most likely involve the non-Markovian dynamics[16, 17]. In our previous work[14], the non-equilibrium effect of the QPC on the qubit dynamics was studied by treating the fermi energy fluctuation of the QPC reservoirs perturbatively. In this paper, a fully non-equilibrium theory describing the qubit decoherence by the QPC measurement is developed using Schwinger-Keldysh's approach[18].

Historically, the Schwinger-Keldysh's approach is well developed to systematically treat the non-equilibrium dynamics of a many-body system.[19, 20, 21] For electron transports in nano-devices, this approach has been used to study the transport current fluctuation and the full counting statistics in the single-electron transistor[21, 22], the current fluctuation in Kondo system[23, 24, 25], and the noise spectrum in the QPC measurement of the charge qubit[26]. To treat the non-equilibrium effect of the electrical reservoir, literaturely the real-time diagrammatic technique was constructed to diagrammatically calculate correlation functions of the electrical reservoir order by order.[21, 24] For the investigation of the non-Markovian dynamics in our system, an alternative real-time diagrammatic technique is developed. The master equation for the charge qubit dynamics is derived and expressed in terms of all orders irreducible diagrams to all orders. The non-Markovian processes in the qubit dynamics can be fully taken into account. The effect of the time variated reservoir fluctuation on the qubit dynamics can then be explicitly studied in this formulism.

In addition, the assumption of the constant hopping amplitude of tunneling electrons across the QPC barrier together with a constant density of state of the QPC reservoirs is usually utilized to specify the QPC structure related to the two reservoirs band structure coupling to the two metal gates. It eventually leads to the

qubit dynamics in the Markovian limit.[11, 12, 13, 14] However, the QPC structure determines the correlation time scale of the tunneling electron fluctuation in the QPC. The non-Markovian processes of the qubit dynamics can emerge if a particular design of the QPC structure is taken into account. We will consider in this work a Lorentzian-type spectral density to characterize the energy-level dependence of the hopping amplitude and the density of state. A close relation between the qubit decoherence and the time correlation of the tunneling-electron fluctuation shows that the qubit decoherence can be controlled through the measurement operation itself.

We organize the paper as follows: The theory of the charge qubit measurement is presented in Sec. II. The real-time diagrammatic technique based on Schwinger-Keldysh's approach are developed in Sec. III, where we also derive the master equation for the reduced density operator of the charge qubit. In Sec IV, the qubit dynamics is studied based on the master equation. The influence of random electron-tunneling processes on the qubit decoherence is illustrated in this section. Finally, a summary is given in Sec V.

II. CHARGE QUBIT MEASUREMENT

The charge qubit measurement using QPC is studied in the tunnel junction regime[8, 10, 11, 12, 13, 14, 26]. In this regime, the transmissions of all tunneling channels cross the QPC barrier are small enough such that the electron tunneling becomes sensitive to the qubit state. The qubit information can then be extracted from the output signal of the QPC, while the backreaction of the measurement to the qubit states is expected to be minimum. The Hamiltonian of the whole system is given by[8, 10, 11, 12, 13, 14, 26]

$$H = H_S + H_B + H', \tag{1}$$

where H_S denotes the Hamiltonian of the charge qubit, H_B the Hamiltonian of the QPC with the electrical reservoirs consisting of the source indexed by l and the drain by r. The charge qubit state is measured through the electron tunneling across the source and the drain. H' is the interaction Hamiltonian describing the electron tunneling processes through the QPC with a qubit-state dependent hopping amplitude q_{rl}. Explicitly,

$$H_S = \frac{\epsilon}{2}\sigma_z + \frac{\triangle}{2}\sigma_x, \tag{2}$$

$$H_B = \sum_l \epsilon_l a_l^+ a_l + \sum_r \epsilon_r a_r^+ a_r, \tag{3}$$

$$H' = \sum_{rl} (q_{rl} a_r^+ a_l + q_{lr} a_l^+ a_r). \tag{4}$$

We shall formulate the non-equilibrium theory of the electron tunnelings coupled with the qubit dynamics in the electron-hole representation, in which H_B and H' can be written equivalently as

$$\begin{aligned} H_B &= \sum_{l>0} (\epsilon_l^e \alpha_l^+ \alpha_l + \epsilon_l^h \beta_l^+ \beta_l) \\ &\quad + \sum_{r>0} (\epsilon_r^e \alpha_r^+ \alpha_r + \epsilon_r^h \beta_r^+ \beta_r), \end{aligned} \tag{5}$$

$$\begin{aligned} H' &= \sum_{rl>0} q_{rl} (\alpha_r^+ \alpha_l + \beta_r \beta_l^+ + \beta_r \alpha_l \\ &\quad + \alpha_r^+ \beta_l^+) + \text{H.c.}, \end{aligned} \tag{6}$$

where $\alpha_{l,r}^+(\alpha_{l,r})$ and $\beta_{l,r}^+(\beta_{l,r})$ are respectively the creation (annihilation) operators of the electron and hole, the corresponding electron and hole energies $\epsilon_{l,r}^e = \epsilon_{l,r} - \mu_{L,R}$ and $\epsilon_{l,r}^h = \mu_{L,R} - \epsilon_{l,r}$ with respect to the chemical potential μ_L of the source and μ_R of the drain. Since the coupling q_{rl} depends on the qubit state, it is indeed a coupling function of the qubit operator. Meanwhile, q_{rl} also depends on the measurement device structure. We remain the discussion of the QPC measurement to the qubit decoherence with a practical q_{rl} later.

The qubit dynamics is determined by the master equation for the reduced density operator $\rho_S(t) = \text{Tr}_B[\rho_{tot}(t)]$, where $\rho_{tot}(t)$ is the total density operator of the whole system, and the partial trace Tr_B integrates over all the degrees of freedom of the QPC reservoir. From the Liouville equation $\frac{\partial}{\partial t}\rho_{tot} = -i[H, \rho_{tot}]$ for the total density operator, it can be shown that the reduced density operator $\rho_S(t)$ obeys the following equation of motion (the master equation) [17, 27, 28]

$$\begin{aligned} \frac{\partial}{\partial t}\rho_S(t) &= -i[H_S, \rho_S(t)] - i\text{Tr}_B\Big[L' Q_{H_0}(t-t_0) \\ &\quad \times \rho_{tot}(t_0)\Big] - \int_{t_0}^{t} d\tau K(t-\tau) * \rho_S(\tau), \end{aligned} \tag{7}$$

where $K(t-\tau) * \rho_S(\tau) \equiv \text{Tr}_B[L' Q_{H_0}(t-\tau) L' \rho_{tot}(\tau)]$, $L' \equiv [H',]$, $Q_{H_0}(t) = e^{-it[H_S + H_B,]}$, and t_0 is the initial time that the interaction between the qubit and the QPC measurement turns on. The derivation of Eq. (7) can be found in Appendix A. The second term in the above equation has no contribution due to the particle number conservation in electron tunneling processes. Since the QPC output signal records the information of the qubit state through the interaction between the QPC and the qubit, the induced backreaction from the fluctuant reservoirs will result in qubit decoherence which is in principle non-Markovian. The non-Markovian dynamics of the qubit is described by the term $-\int_{t_0}^{t} d\tau K(t-\tau) * \rho_S(\tau)$, which contains all influences of the fluctuant reservoir to the qubit dynamics. The qubit decoherence is thus totally governed by Eq. (7). In the following discussion, we will derive the master equation for the reduced density operator in terms of a diagrammatic perturbation expansion of Eq. (7).

III. REAL-TIME DIAGRAMMATIC TECHNIQUE

We begin with the Schwinger-Keldysh's approach[18] to explicitly calculate the term $-\int_{t_0}^{t} d\tau K(t-\tau)*\rho_S(\tau)$ in Eq. (7). In the interaction picture, the interaction Hamiltonian Eq. (6) can be rewritten as

$$\hat{H}'_t = \sum_{rl>0} \left\{ \hat{q}_{rl}(t)\hat{\psi}^+_r(t)\hat{\psi}_l(t) + \hat{q}^+_{rl}(t)\hat{\psi}^+_l(t)\hat{\psi}_r(t) \right\}, \quad (8)$$

where the field operator $\hat{\psi}_k(t)$ is defined by

$$\hat{\psi}_k(t) = \alpha_k e^{-i\epsilon^e_k(t-t_0)} + \beta^+_k e^{i\epsilon^h_k(t-t_0)} \quad (9)$$

with the index $k = l, r$ labeled respectively for the source and the drain. In addition, $K(t-\tau)*\rho_S(\tau)$ in the interaction picture can be rewritten as

$$\begin{aligned} & K(t-\tau)*\rho_S(\tau) = Q_S(t-t_0) \\ & \times \Big(\mathrm{Tr}_B \left[\hat{H}'_t \hat{H}'_\tau T_{\tilde{p}} \left\{ e^{-i\int_{\tilde{p},t_0}^{\tau} ds \hat{H}'_s} \rho_{tot}(t_0) \right\} \right] \\ & - \mathrm{Tr}_B \left[\hat{H}'_t T_{\tilde{p}} \left\{ e^{-i\int_{\tilde{p},t_0}^{\tau} ds \hat{H}'_s} \rho_{tot}(t_0) \right\} \hat{H}'_\tau \right] \\ & - \mathrm{Tr}_B \left[\hat{H}'_\tau T_{\tilde{p}} \left\{ e^{-i\int_{\tilde{p},t_0}^{\tau} ds \hat{H}'_s} \rho_{tot}(t_0) \right\} \hat{H}'_t \right] \\ & + \mathrm{Tr}_B \left[T_{\tilde{p}} \left\{ e^{-i\int_{\tilde{p},t_0}^{\tau} ds \hat{H}'_s} \rho_{tot}(t_0) \right\} \hat{H}'_\tau \hat{H}'_t \right] \Big), \end{aligned} \quad (10)$$

where $Q_S(t) = e^{-it[H_S,]}$ and $\int_{\tilde{p},t_0}^{t} ds$ denotes the closed-time-path integral along the closed-time-path contour $\tilde{p}$ [18, 19, 20, 21] with the range of the real time axis from t_0 to t. The closed time path contains the positive branch and the negative branch. The positive branch coincides with the real time axis, and the negative branch is reversed with respect to the real time axis. Taking perturbation expansion of Eq. (10)

$$\begin{aligned} K(t-\tau)*\rho_S(\tau) = & K^{(0)}(t-\tau)*\rho_S(\tau) \\ & + K^{(1)}(t-\tau)*\rho_S(\tau) + \cdots \end{aligned} \quad (11)$$

through the expansion[19]

$$\begin{aligned} T_{\tilde{p}} \left\{ e^{-i\int_{\tilde{p}} ds \hat{H}'_s} \rho_{tot}(t_0) \right\} = & \sum_{n=0}^{\infty} \frac{(-i)^n}{n!} \int_{\tilde{p}} ds_1 \cdots \int_{\tilde{p}} ds_n \\ & \times T_{\tilde{p}} \left\{ \hat{H}'_{s_1} \cdots \hat{H}'_{s_n} \rho_{tot}(t_0) \right\}, \end{aligned} \quad (12)$$

we can diagrammatically illustrate Eq. (10) as

$K(t-\tau)*\rho_S(\tau)$

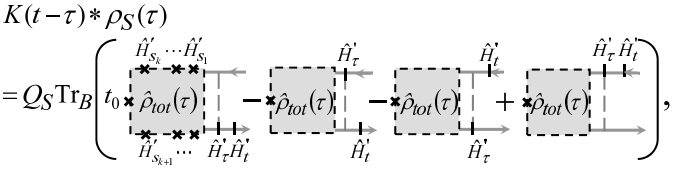

$$\text{with} \quad \hat{\rho}_{tot}(\tau) = T_{\tilde{p}} \left\{ e^{-i\int_{\tilde{p},t_0}^{\tau} ds \hat{H}'_s} \rho_{tot}(t_0) \right\}. \quad (13)$$

According to the Wick's theorem, all higher order correlation functions of the fermion field operators can be built up in terms of the unperturbed Green's function.[19, 20, 21] The reservoir contour-ordered Green's function is defined by

$$\tilde{G}_k(t,t') = -i \left\langle T_{\tilde{p}} \Big(\hat{\psi}_k(t) \hat{\psi}^+_k(t') \Big) \right\rangle, \quad (14)$$

where the contour-ordering operator $T_{\tilde{p}}$ orders the operator $\hat{\psi}_k(t)\hat{\psi}^+_k(t')$ according to their time arguments along the $\tilde{p}$, and $\langle . \rangle$ denotes the non-equilibrium statistical average. Explicitly, $\tilde{G}_k(t,t')$ contains four components:

$$\tilde{G}_k(t,t') = \begin{pmatrix} G_{F,k}(t,t') & G_{<,k}(t,t') \\ G_{>,k}(t,t') & G_{\tilde{F},k}(t,t') \end{pmatrix}, \quad (15)$$

i.e. the time-ordered Green's function $G_{F,k}$, the anti-time-ordered Green's function $G_{\tilde{F},k}$, the correlation Green's functions $G_{<,k}(t,t')$ and $G_{>,k}$, defined respectively as

$$G_{F,k}(t,t') = -i \left\langle T(\hat{\psi}_k(t)\hat{\psi}^+_k(t')) \right\rangle, \quad (16)$$

$$G_{\tilde{F},k}(t,t') = -i \left\langle \tilde{T}(\hat{\psi}_k(t)\hat{\psi}^+_k(t')) \right\rangle, \quad (17)$$

$$G_{<,k}(t,t') = i \left\langle \hat{\psi}^+_k(t')\hat{\psi}_k(t) \right\rangle, \quad (18)$$

$$G_{>,k}(t,t') = -i \left\langle \hat{\psi}_k(t)\hat{\psi}^+_k(t') \right\rangle, \quad (19)$$

where T is the normal time-ordering operator and $\tilde{T}$ the anti-time-ordering operator. The unperturbed reservoir contour-ordered Green's functions are easy calculated,

$$\begin{aligned} -iG^{(0)}_{<,k}(t,t') &= \mathrm{Tr}_B \left[\hat{\psi}^+_k(t')\hat{\psi}_k(t)\rho^{(0)}_B \right] \\ &= \Big(1 - f(\epsilon^h_k)\Big) e^{i\epsilon^h_k(t-t')} \\ &\quad + f(\epsilon^e_k) e^{-i\epsilon^e_k(t-t')}, \end{aligned} \quad (20)$$

$$\begin{aligned} iG^{(0)}_{>,k}(t,t') &= \mathrm{Tr}_B \left[\hat{\psi}_k(t)\hat{\psi}^+_k(t')\rho^{(0)}_B \right] \\ &= \Big(1 - f(\epsilon^e_k)\Big) e^{-i\epsilon^e_k(t-t')} \\ &\quad + f(\epsilon^h_k) e^{i\epsilon^h_k(t-t')}, \end{aligned} \quad (21)$$

$$G^{(0)}_{F,k}(t,t') = \theta(t-t')G^{(0)}_{>,k}(t,t') + \theta(t'-t)G^{(0)}_{<,k}(t,t'), \quad (22)$$

$$G^{(0)}_{\tilde{F},k}(t,t') = \theta(t-t')G^{(0)}_{<,k}(t,t') + \theta(t'-t)G^{(0)}_{>,k}(t,t'), \quad (23)$$

Here, the electrical reservoirs are assumed to be in the thermal equilibrium state $\rho^{(0)}_B$ initially (at t_0), and $f(\epsilon)$ is the Fermi-Dirac distribution function. These Green's functions describe the contractions of the unperturbed fermion pair with four different time contour-orderings.

A. The diagrammatic rules

In order to systematically trace out the reservoir degrees of freedom to all orders in the perturbation expansion with a correct operator ordering for the remaining degrees of freedom of the qubit, we shall use the real-time diagrammatic expansion with the diagrammatic rules defined as follows: According to the interaction Hamiltonian of Eq. (8), two kinds of the tunnelings, the forward and the backward tunneling, across the QPC barrier are involved. The diagrammatic representation of the forward tunneling vertex $\hat{q}_{rl}\hat{\psi}_r^+\hat{\psi}_l$ and the backward tunneling vertex $\hat{q}_{rl}^+\hat{\psi}_l^+\hat{\psi}_r$ are depicted in Fig. 1 (a). For the forward tunneling vertex, the incoming dashed line labeled by l represents the electrons (or holes) above (below) the chemical potential μ_L are destroyed (created) in the source, and the outgoing solid line labeled by r represents the electrons (or holes) with the energy level above (below) the chemical potential μ_R are created (destroyed) in the drain. The QPC current due to this tunneling effectively flows from the source to the drain. The coupling operator $\hat{q}_{rl}$ is presented in the vertex with a filled circle for the forward tunneling. Similarly, the interaction associated with the backward tunneling is depicted by the incoming solid line labeled by r and the outgoing dashed line labeled by l, and the coupling operator $\hat{q}_{rl}^+$ presented in the vertex is denoted with a hollow circle.

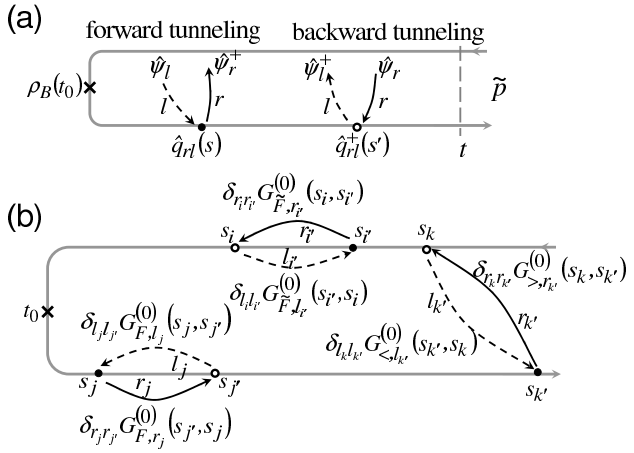

FIG. 1: The diagrammatic representation. (a) The forward tunneling vertex $\hat{q}_{rl}(t)\hat{\psi}_r^+(t)\hat{\psi}_l(t)$ and the backward tunneling vertex $\hat{q}_{lr}(t)\hat{\psi}_l^+(t)\hat{\psi}_r(t)$. (b) The free propagators.

Meanwhile, all vertices in the expansion should be connected in pairs by the electron propagators. There are only two types of the propagators involved: the solid line, starting from the vertex $\hat{q}_{rl}\hat{\psi}_r^+\hat{\psi}_l$ to the vertex $\hat{q}_{rl}^+\hat{\psi}_l^+\hat{\psi}_r$, represents the electron propagates in the drain, and the dash line, starting from the vertex $\hat{q}_{rl}^+\hat{\psi}_l^+\hat{\psi}_r$ to the vertex $\hat{q}_{rl}\hat{\psi}_r^+\hat{\psi}_l$, is the propagator in the source. These propagators connecting two vertices with both the time arguments s and s' located at the positive (negative) branch of the closed time path represent the (anti-) time-ordered Green's function $G^{(0)}_{F(\tilde{F})}(s,s')$. The arrow of the propagator coincides with the propagating direction of the tunneling electron. While the propagator connecting two vertices, one located at the positive branch and the other at the negative branch separately, represents the correlation Green's function $G^{(0)}_{<(>)}(s,s')$ with respect to the arrow pointing to the vertex at the positive (negative) branch. The diagrammatic representation of the free propagators is summarized in Fig. 1 (b). Different from the usual closed-time-path contour used in the literature, we choose an alternate contour $\tilde{p}$ depicted in Fig. 1. The lower (upper) axis represents the positive (negative) time branch of the closed-time-path contour. The contour ordering $t \geq_{\tilde{p}} t'$ denotes the time t' is former than t along the arrow of the contour $\tilde{p}$, and the corresponding operator $\hat{q}(t')$ is applied earlier than $\hat{q}(t)$. This prescription makes the calculation more convenient in the treatment of the time ordering of coupling operators discussed below.

B. The real-time diagrammatic expansion

Now, we can diagrammatically calculate the partial trace in the expansion of Eq. (10)

$$\mathrm{Tr}_B\left[T_{\tilde{p}}\left\{\hat{H}'_t\hat{H}'_\tau\hat{H}'_{s_1}\cdots\hat{H}'_{s_n}\rho_{tot}(t_0)\right\}\right], \tag{24}$$

where $\hat{H}'_{s_1}\cdots\hat{H}'_{s_n}$ comes from the perturbation expansion of the evolution operator $T_{\tilde{p}}\{\exp(-i\int_{\tilde{p},t_0}^{\tau} ds\hat{H}'_s)\cdot\}$ with $t \geq \tau \geq (s_1,\cdots,s_n)$. Conveniently, the vertex with the time argument $s_{i=1,\cdots,n}$ is called the internal vertex and that with (t,τ) is called the external vertex. The time contour ordering $T_{\tilde{p}}$ in Eq. (24) comprises all the permutation of the time series $\{t \geq \tau \geq (s_1,\cdots,s_n)\}$ along the closed time path $\tilde{p}$, namely, one must sum all allowed time contour orderings $T_{\tilde{p}} = \sum_i T_{\tilde{p},i}$. In terms of $\hat{q}_{rl}\hat{\psi}_r^+\hat{\psi}_l$ and $\hat{q}_{rl}^+\hat{\psi}_l^+\hat{\psi}_r$, each component of Eq. (24) can be expressed as

$$\begin{aligned}
&\mathrm{Tr}_B\Big[T_{\tilde{p}}\Big\{\Big(\hat{q}_{rl}(t)\hat{\psi}_r^+(t)\hat{\psi}_l(t)\Big)^{(+)}\\
&\qquad\times\Big(\hat{q}_{r'l'}(\tau)\hat{\psi}_{r'}^+(\tau)\hat{\psi}_{l'}(\tau)\Big)^{(+)}\cdots\\
&\qquad\times\Big(\hat{q}_{r_nl_n}(s_n)\hat{\psi}_{r_n}^+(s_n)\hat{\psi}_{l_n}(s_n)\Big)^{(+)}\rho_{tot}(t_0)\Big\}\Big]\\
&=\sum_i \mathcal{E}_{rlr'l'\cdots r_nl_n;i}\mathcal{S}_{rlr'l'\cdots r_nl_n;i},
\end{aligned} \tag{25}$$

where $\mathcal{S}_{rlr'l'\cdots r_nl_n;i}$ associated with coupling operators is defined as

$$\begin{aligned}
&\mathcal{S}_{rlr'l'\cdots r_nl_n;i}(t,\tau,s_1,\cdots,s_n)\\
&\equiv T_{\tilde{p},i}\left\{\hat{q}_{rl}^{(+)}(t)\hat{q}_{r'l'}^{(+)}(\tau)\hat{q}_{r_1l_1}^{(+)}(s_1)\cdots\hat{q}_{r_nl_n}^{(+)}(s_n)\rho_S(t_0)\right\},
\end{aligned} \tag{26}$$

and the corresponding coefficient $\mathcal{E}_{rlr'l'\cdots r_n l_n;i}$ is the contribution of integrating out the electron reservoirs and is defined by

$$\begin{aligned}
&\mathcal{E}_{rlr'l'\cdots r_n l_n;i}(t,\tau,s_1,\cdots,s_n)\\
\equiv\ &\mathrm{Tr}_B\Big[T_{\tilde{p},i}\Big\{(\hat{\psi}^+_r(t)\hat{\psi}_l(t))^{(+)}(\hat{\psi}^+_{r'}(\tau)\hat{\psi}_{l'}(\tau))^{(+)}\cdots\\
&\times(\hat{\psi}^+_{r_n}(s_n)\hat{\psi}_{l_n}(s_n))^{(+)}\rho_B^{(0)}\Big\}\Big]. \qquad (27)
\end{aligned}$$

Note that $\mathcal{S}_{rl\cdots;i}$ in Eq. (26) consists of $n+2$ vertices which is ordered according to $T_{\tilde{p},i}$. Due to the particle number conservation in electron tunneling processes, only even orders (n =even) in the perturbation expansion have contribution. Half of these $n+2$ vortices will carry with the coupling operator $\hat{q}^+$, and the others with $\hat{q}$. Each $\mathcal{E}_{rl\cdots;i}\mathcal{S}_{rl\cdots;i}$ is expressed by a set of topology-independent diagrams, in which each diagram are composed of several allowed closed loops connecting $n+2$ vertices. The topology-independence means the order and the direction of all propagators lines and the loop assembly are different. The coefficient $\mathcal{E}_{rl\cdots;i}$ can be directly calculated only from this set of topology-independent diagrams by summing all the topology-independent diagrams with a prefactor $(-1)^{(n+2)/2+l}$, where l is the loop number in the individual topology-independent diagram. The prefactor $(-1)^{(n+2)/2}$ comes from the factor $(-i)^{(n+2)}$ of the n-th order perturbation, and the prefactor $(-1)^l$ is due to the permutation between the fermion operators in the contraction. An explicit example of calculating $\mathcal{E}_{rl\cdots;i}\mathcal{S}_{rl\cdots;i}$ for the order of $n=2$ can be found in Appendix B.

Accordingly, we introduce a loop operator $\hat{\mathcal{L}}_\tau(\cdots)$ to calculate the total contribution of all time contour orderings in the n-th order perturbation $K^{(n)}(t-\tau)*\rho_S(\tau)$. This loop operator is defined by a loop in particular topology-independent diagrams along *the real time axis*,

$$\begin{aligned}
&\hat{\mathcal{L}}_\tau\begin{pmatrix} s_1 & s_2 & s_3 & \cdots s_i\cdots & s_{2p} & s_1\\ k_1 & k_1' & k_2 & \cdots k_j\cdots\ k_p & k_p' & \end{pmatrix}\\
\equiv\ &\sum_{k_1\cdots k_p}\sum_{k_1'\cdots k_p'}\int_{t_0}^{\tau}ds_1\cdots\int_{t_0}^{\tau}ds_{2p}\\
&\times\mathrm{Tr}\Big[D[\alpha_{k_1}(s_1)]\tilde{G}^{(0)}_{k_1}(s_1,s_2)D[\alpha_{k_1'}(s_2)]\tilde{G}^{(0)}_{k_1'}(s_2,s_3)\\
&\cdots D[\alpha_{k_p'}(s_{2p})]\tilde{G}^{(0)}_{k_p'}(s_{2p},s_1)\Big], \qquad (28)
\end{aligned}$$

where $s_{i=1,\cdots,2p}\le\tau$ are the time arguments of the internal vertices, p is an integer with $2p\le n$, k_j and k_j' are the energy indexes with ($k_j=l_j,k_j'=r_j$) or ($k_j=r_j,k_j'=l_j$), $\tilde{G}^{(0)}_k(s,s')$ is the Keldysh's matrix shown in Eq. (15), and the 2×2 functional-derivative matrix $D[\alpha(s)]$ is defined by $D[\alpha(s)]=\begin{pmatrix}\frac{\delta}{\delta\alpha(s)} & 0\\ 0 & \frac{\delta}{\delta\alpha^*(s)}\end{pmatrix}$ with $\alpha(s)$ being a time-dependent parameter. The loop involving the external vertices is denoted as $\hat{\mathcal{L}}_\tau\begin{pmatrix} t & s_1 & \cdots\tau\cdots & s_{2p-2} & t\\ k_1 & & \cdots k_j\cdots & & k_p'\end{pmatrix}$. This definition is the same as Eq. (28) but without taking the time integral for the time arguments t and τ. The loop operator is written in such a way that a pair of vertices labeled by the time arguments s' and s together with the propagator with the energy index k represent a segment of the loop operator $\hat{\mathcal{L}}_\tau\begin{pmatrix}\cdots s' & s\cdots\\ & k\end{pmatrix}$. Each internal (external) vertex with the coupling operator $\hat{q}_{rl}$ or $\hat{q}^+_{rl}$ is described by the operator $D[\alpha_l]$ ($D[\gamma_l]$) and $D[\alpha_r]$ ($D[\gamma_r]$), respectively. The connecting propagator is the Keldysh's matrix $\tilde{G}^{(0)}_k(s,s')$. Along the propagating direction in each loop, the corresponding loop operator is written down in the order from right to left. The loop is end-point-independent, with which the definition of the loop operator coincides. Since the hermitian of the physical quantity, $K^{(n)}(t-\tau)*\rho_S(\tau)$ can be separated into two parts which are hermitian conjugate to each other. This leads to two sets of the diagrams which are dual each other. The duality of two diagrams is defined that the replacements of the vertices $\hat{q}$ ($\hat{q}^+$) in one diagram by the vertices $\hat{q}^+$ ($\hat{q}$) equals to each other. Therefore, we only need to calculate one set of the diagrams. In terms of the loop operators, only topology-independent diagrams along the real time axis should be taken into account. Furthermore, besides the prefactor $\frac{1}{n!}(-1)^{(n+2)/2+l}$, where the factor $\frac{1}{n!}$ comes from the n-th order perturbation, a weight factor (the number of topology-equivalent diagrams) should also be added for each topology-independent diagram to calculate $K^{(n)}(t-\tau)*\rho_S(\tau)$ correctly.

Meanwhile, each order of the kernel expansion $K^{(n)}(t-\tau)*\rho_S(\tau)$ in Eq. (11) contains multi-particle ($2,4,\cdots,n+2$ particles) correlations. We can re-express the perturbation expansion of $K(t-\tau)*\rho_S(\tau)$ in terms of the irreducible diagrams

$$\begin{aligned}
&K(t-\tau)*\rho_S(\tau)\\
=\ &K^{(0)}_{ir}(t-\tau)*\rho_S(\tau)+K^{(2)}_{ir}(t-\tau)*\rho_S(\tau)+\cdots. \qquad (29)
\end{aligned}$$

Explicitly, the n-th order perturbation $K^{(n)}_{ir}(t-\tau)*\rho_S(\tau)$ contains $n+2$ vertices with the time arguments $\{t,\tau,s_1,\cdots,s_n\}$. All vertices are denoted by filled circles without discriminating $\hat{q}$ and $\hat{q}^+$. Also, n internal vertices are treated indistinguishably, namely, a diagram which exchanges arbitrary two time arguments of internal vertices is topology-invariant. The counterclockwise and clockwise loops through the same vertices are also equivalent except that the vertex orderings along the both loop are different. Thus, we define *irreducible diagrams* as all *connected* topology-independent diagrams. The connected diagram means that each loop of the diagram should intersect with other loops at least once. As a result, $K^{(n)}_{ir}(t-\tau)*\rho_S(\tau)$ comprises all irreducible diagrams with the prefactor $(-1)^{(n+2)/2+l}$. Each loop of irreducible diagrams is then given by the irreducible loop

operator defined as follows:

$$\begin{aligned}
&\hat{\mathcal{L}}_{ir,\tau}\left(\begin{array}{ccccccc} t & , & s_1 & , \cdots \tau \cdots s_i \cdots , & s_{2p-2} & , & t \end{array}\right) \\
&= \hat{\mathcal{L}}_{\tau}\left(\begin{array}{ccccccc} t & & s_1 & \cdots \tau \cdots s_i \cdots & s_{2p-2} & & t \\ & l_1 & & \cdots & & r_p & \end{array}\right) \\
&\quad +\hat{\mathcal{L}}_{\tau}\left(\begin{array}{ccccccc} t & & s_{2p-2} & \cdots s_i \cdots \tau \cdots & s_1 & & t \\ & r_p & & \cdots & & l_1 & \end{array}\right).
\end{aligned} \tag{30}$$

The loop operators up to the second order perturbation can be easily calculated accordingly, see Appendix C. The explicit result of the irreducible diagrams and the corresponding loop operators is shown in Fig. 2.

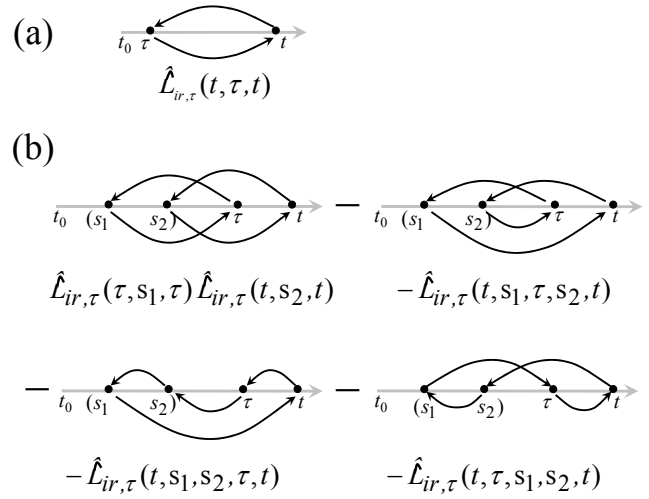

FIG. 2: Irreducible diagrams and the corresponding loop operators. (a) and (b) The leading and the second order contributions.

C. Master equation for the reduced density operator

Thus, writing down the corresponding loop operators one by one according to the resulted irreducible diagrams, and applying these irreducible loop operators to the following generating functional

$$\begin{aligned}
\mathcal{J}(\hat{q},\hat{q}^+;\vec{\alpha},\vec{\gamma}) = \int dt' \mathcal{C}[\vec{\gamma}(t')] \int d\tau' \mathcal{C}[\vec{\gamma}'(\tau')] \\
\times \mathcal{J}_{in}(\hat{q},\hat{q}^+;\vec{\alpha}),
\end{aligned} \tag{31}$$

$$\begin{aligned}
\mathcal{C}[\vec{\gamma}(t)](\cdot) &= \Big\{\gamma_l(t)\hat{q}_{rl}(t)(\cdot) - \gamma_l^*(t)(\cdot)\hat{q}_{rl}(t)\Big\} \\
&\quad +\Big\{\gamma_r(t)\hat{q}^+_{rl}(t)(\cdot) - \gamma_r^*(t)(\cdot)\hat{q}^+_{rl}(t)\Big\},
\end{aligned} \tag{32}$$

$$\begin{aligned}
&\mathcal{J}_{in}(\hat{q},\hat{q}^+;\vec{\alpha}) \\
&= Te^{-i\int ds\{\alpha_l(s)\hat{q}_{rl}(s)+\alpha_r(s)\hat{q}^+_{rl}(s)\}}\rho_S(t_0) \\
&\quad \times\tilde{T}e^{i\int ds'\{\alpha_l^*(s')\hat{q}_{rl}(s')+\alpha_r^*(s')\hat{q}^+_{rl}(s')\}},
\end{aligned} \tag{33}$$

and then taking all parameters $(\alpha(s),\gamma(s))$ to be zero, the explicit expression of $K_{ir}^{(n)}(t-\tau)*\rho_S(\tau)$ can be obtained in terms of coupling operators. Here, the functional derivatives $\left\{\frac{\delta}{\delta\alpha^{(*)}}\cdots\frac{\delta}{\delta\gamma^{(*)}}\right\}$ in irreducible loop operators are responsible to generate the correct orderings of the coupling operators, namely, $\{\mathcal{S}_{rlr'l'\cdots r_n l_n;i}\}$.

As a result, we obtain the master equation for the reduced density operator expressed in terms of the irreducible loop operators to all orders in perturbation expansions,

$$\frac{\partial}{\partial t}\rho_S(t) = -i\left[H_S,\rho_S(t)\right] - \int_{t_0}^{t} d\tau K(t-\tau)*\rho_S(\tau), \tag{34}$$

$$\begin{aligned}
&K(t-\tau)*\rho_S(\tau) = Q_S(t-t_0) \\
&\times\Big\{\hat{\mathcal{K}}_{ir}(t,\tau)\cdot e^{\hat{\mathcal{W}}(\tau)}\cdot\mathcal{J}(\hat{q},\hat{q}^+;\vec{\alpha},\vec{\gamma})\Big\}\Big|_{\vec{\gamma}=\vec{\gamma}'=\{\vec{\alpha}\}=0},
\end{aligned} \tag{35}$$

where $\hat{\mathcal{K}}_{ir}(t,\tau)$ consists of all allowed irreducible diagrams (in terms of the irreducible loop operators)

$$\begin{aligned}
\hat{\mathcal{K}}_{ir}(t,\tau) &= \sum_{n=0}^{\infty}(-1)^n\hat{\mathcal{L}}_{ir,\tau}\left(t,\mathbf{P}_\tau\{\tau,s_1,\cdots,s_{2n}\},t\right) \\
&+ \sum_{n,n'=0}^{\infty}(-1)^{n+n'}\hat{\mathcal{L}}_{ir,\tau}\left(\tau,s_1',\cdots,s_{2n'+1}',\tau\right) \\
&\times\hat{\mathcal{L}}_{ir,\tau}\left(t,s_1,\cdots,s_{2n+1},t\right)
\end{aligned} \tag{36}$$

with $\mathbf{P}_\tau\{\tau,s_1,s_2,s_3,\cdots,s_n\} = \{\tau,s_1,s_2,s_3,\cdots\} + \{s_1,\tau,s_2,s_3,\cdots\} + \cdots$ containing $n+1$ permutations, and the operator $\hat{\mathcal{W}}(t)$ is defined as

$$\hat{\mathcal{W}}(t) = \sum_{n=1}^{\infty}\frac{(-1)^{n+1}}{n}\hat{\mathcal{L}}_{in,\tau}[s_1,\cdots s_{2n},s_1], \tag{37}$$

a log form in the Taylor expansion, and the loop operator $\hat{\mathcal{L}}_{in,\tau}[\cdots]$ only involving the internal vertices is given by

$$\begin{aligned}
&\hat{\mathcal{L}}_{in,\tau}[\ s_1\ ,\cdots s_{2p},\ s_1\ ] \\
&\equiv \frac{1}{2}\hat{\mathcal{L}}_{ir,\tau}\left(\ s_1\ ,\cdots s_{2p},\ s_1\ \right). \\
&= \hat{\mathcal{L}}_{\tau}\left(\begin{array}{ccccccc} s_1 & & s_2 & \cdots & s_{2p} & & s_1 \\ & k_1 & & \cdots & & k_p' & \end{array}\right) \\
&= \hat{\mathcal{L}}_{\tau}\left(\begin{array}{ccccccc} s_1 & & s_{2p} & \cdots & s_2 & & s_1 \\ & k_p' & & \cdots & & k_1 & \end{array}\right).
\end{aligned} \tag{38}$$

In fact, the operator $e^{\hat{\mathcal{W}}(t)}$ generates all the loop operators for the reduced density operator $\rho_S(\tau)$:

$$\rho_S(t) = Q_S(t-t_0)\Big\{e^{\hat{\mathcal{W}}(t)}\mathcal{J}_{in}(\hat{q},\hat{q}^+;\vec{\alpha})\Big|_{\{\vec{\alpha}\}=0}\Big\}. \tag{39}$$

The leading order contribution ($n = 0$) to the master equation is obtained as follows

$$\frac{\partial}{\partial t}\rho_S(t) = -i\left[H_S, \rho_S(t)\right] - Q_S(t-t_0) \times \int_{t_0}^{t} d\tau K_{ir}^{(0)}[t-\tau, \rho_S(\tau)], \quad (40)$$

$$K_{ir}^{(0)}[t-\tau, \rho_S(\tau)] = \Big\{\hat{\mathcal{L}}_{ir,\tau}\left(t,\tau,t\right)\int dt'\mathcal{C}[\vec{\gamma}(t')] \times \int d\tau'\mathcal{C}[\vec{\gamma}'(\tau')]Q_S^{-1}(\tau-t_0)\rho_S(\tau)\Big\}\Big|_{\vec{\gamma}=\vec{\gamma}'=0}. \quad (41)$$

Also, the time variated reservoir fluctuation due to the interaction with the qubit has been taken into account. The internal vertices of $\hat{\mathcal{K}}_{ir}(t,\tau)$ and $e^{\hat{\mathcal{W}}(\tau)}$ in Eq. (35) are mixed together for higher order contributions. The reduced density operator can not be extracted unless the following approximation is utilized,

$$\hat{\mathcal{K}}_{ir}(t,\tau)e^{\hat{\mathcal{W}}(\tau)}\mathcal{J}(\hat{q},\hat{q}^+;\vec{\alpha},\vec{\gamma})\Big|_{\vec{\gamma}=\vec{\gamma}'=\{\vec{\alpha}\}=0} \approx \hat{\mathcal{K}}_{ir}(t,\tau)\mathcal{J}_{BA}(\hat{q},\hat{q}^+;\vec{\alpha},\vec{\gamma})\Big|_{\vec{\gamma}=\vec{\gamma}'=\{\vec{\alpha}\}=0}, \quad (42)$$

$$\mathcal{J}_{BA}(\hat{q},\hat{q}^+;\vec{\alpha},\vec{\gamma}) \equiv \int dt'\mathcal{C}[\vec{\gamma}(t')]\int d\tau'\mathcal{C}[\vec{\gamma}'(\tau')] \times Te^{-i\int ds\{\alpha_l(s)\hat{q}_{rl}(s)+\alpha_r(s)\hat{q}_{rl}^+(s)\}} \times \Big\{Q_S^{-1}(\tau-t_0)\rho_S(\tau)\Big\} \times \tilde{T}e^{i\int ds'\{\alpha_l^*(s')\hat{q}_{rl}(s')+\alpha_r^*(s')\hat{q}_{rl}^+(s')\}}. \quad (43)$$

Without resorting the traditional diagrammatic technique in the Laplace space, the real-time diagrammatic technique has been developed to derive the master equation. The charge qubit dynamics in the non-Markovian regime can be studied based on Eqs. (34-41).

IV. QUBIT DECOHERENCE

To explore the qubit decoherence induced by the QPC measurement, the charge qubit as a single electron in a double quantum dots[8] is considered. The Hamiltonian of the system in Eq. (2) can be explicitly written as

$$H_S = E_L c_L^+ c_L + E_R c_R^+ c_R + \Omega_0(c_L^+ c_R + c_R^+ c_L), \quad (44)$$

where $c_L^+(c_L)$ and $c_R^+(c_R)$ are the creation (annihilation) operators of the electron sited in the two dots labeled by L and R with the single-electron constraint $c_L^+c_L + c_R^+c_R = 1$, $E_{L,R}$ are the corresponding energies, and Ω_0 is the electron hopping amplitude between the double dots. The interaction between the system and the QPC due to the measurement is characterized by the interaction coupling[8]

$$q_{rl} = \Omega(\epsilon_l,\epsilon_r) - \Omega'(\epsilon_l,\epsilon_r)c_R^+c_R, \quad (45)$$

and Ω and $\Omega - \Omega'$ in Eq. (45) are the electron hoping amplitude of the QPC without and with the measurement of the single electron in the double dots. Eq. (45) describes a variation in the barrier of the QPC when the single electron occupies on the right dot.

We shall consider the leading order contribution to the master equation. According to Eqs. (40,41), we obtain

$$\frac{\partial}{\partial t}\rho_S(t) = -i\left[H_S,\rho_S(t)\right] - \int_{t_0}^{t} d\tau\Big[R_0,[[k(t-\tau) \times R(t-\tau), e^{-iH_S(t-\tau)}\rho_S(\tau)e^{iH_S(t-\tau)}]]\Big], \quad (46)$$

where the double bracket $[[A,B]] = AB - (AB)^+$, the operator $R(t)$ is given by

$$R(t) = \cos\theta(|e\rangle\langle e| - |g\rangle\langle g|) - \sin\theta(e^{i\gamma t}|g\rangle\langle e| + e^{-i\gamma t}|e\rangle\langle g|) \quad (47)$$

with $\gamma = \sqrt{4\Omega_0^2 + (E_L - E_R)^2}$ the energy difference between the ground state $|g\rangle$ and the excited state $|e\rangle$ of the qubit, $\theta = \cos^{-1}[(E_L - E_R)/\gamma]$, and $R_0 = R(t=0)$. The reservoir correlation function $k(s)$ in Eqs. (46) which characterizes the QPC structure associated with the temperature effect and the external bias is expressed as

$$k(s) = \int_{-\infty}^{\infty}\frac{d\epsilon d\epsilon'}{4\pi^2}e^{i(\epsilon-\epsilon')s}\tilde{k}(\epsilon,\epsilon'), \quad (48)$$

$$\tilde{k}(\epsilon,\epsilon') = f_R(\epsilon)(1-f_L(\epsilon'))J(\epsilon,\epsilon') + f_L(\epsilon)(1-f_R(\epsilon'))J(\epsilon',\epsilon), \quad (49)$$

where $\tilde{k}(\epsilon,\epsilon')$ is the electron-tunneling spectrum for the QPC, $f_{L,R}(\epsilon) = 1/(1+\exp\beta(\epsilon-\mu_{L,R}))$ are respectively the Fermi-Dirac distribution functions for the source and the drain, and the spectral density $J(\epsilon',\epsilon)$ for the QPC structure is given by

$$J(\epsilon,\epsilon') = \pi^2 g_L(\epsilon')g_R(\epsilon)\left|\Omega'(\epsilon,\epsilon')\right|^2 \quad (50)$$

with $g_{L,R}(\epsilon)$ being the density of states of the source and the drain. Also, we assume here the electron energy levels $\{\epsilon_l,\epsilon_r\}$ are continuous. Eq. (46) contains the non-Markovian processes of the qubit dynamics up to the leading order. It can be checked Eq. (46) reduces to the result in Refs. [13, 14] in the Markovian limit.

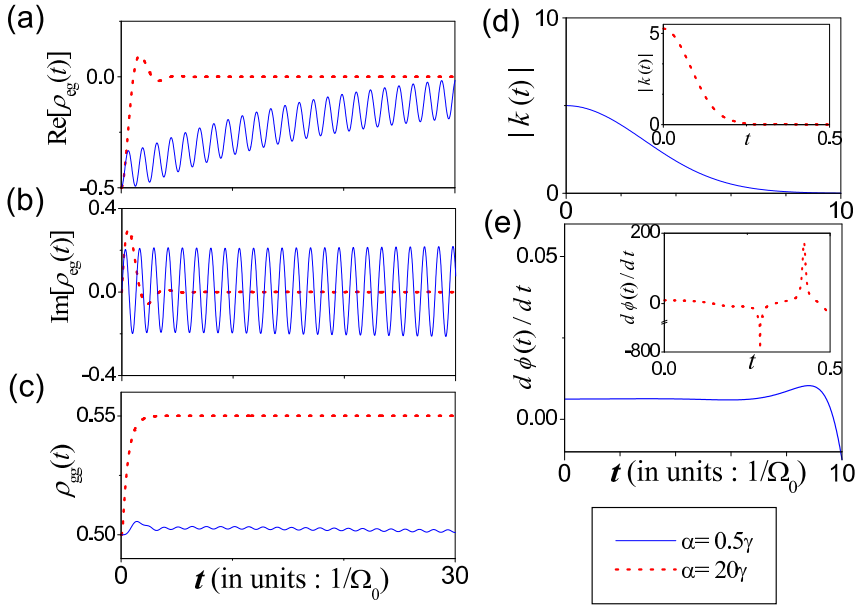

FIG. 3: (color online). The qubit dynamics and the corresponding reservoir time correlation function in the measurement condition with an extreme small w ($w \ll \gamma$) and different α. The symmetric coupled quantum dots ($\gamma = 2\Omega_0$) is simulated. The qubit is set initially in the $|L\rangle$ state. The following measurement parameters are used with Ω_0 being a rescaling factor: $\beta = 1/\Omega_0$, $V_d = 20\Omega_0$ and $p = \Omega_0$. (a) and (b) The qubit dephasing. The time evolution of the real and imaginary parts of the qubit density matrix element ρ_{eg} are plotted, respectively. (c) The qubit relaxation. The time evolution of the qubit density matrix element ρ_{gg} for the qubit in the ground state is plotted. (d) The amplitude of the reservoir time correlation function is plotted in units Ω_0^2. (e) The time derivative of the phase in the reservoir time correlation function is plotted in units Ω_0. The integration in Eq. (56) is approximately calculated by fitting the Lorentzian spectral density with Gaussian function to remove the energy cut-off.

To make the non-Markovian feature apparent, we shall concentrate on the charge qubit with symmetric coupled dots $E_L = E_R$ characterized by $\gamma = 2\Omega_0$ ($\theta = \pi/2$). The equation of motion for the reduced density matrix becomes,

$$\frac{\partial \rho_{eg}(t)}{\partial t} = -i\gamma\rho_{eg}(t) - 2\int_{t_0}^{t} d\tau |k(t-\tau)| \cos\phi(t-\tau) \times\Big\{\rho_{eg}(\tau) - \rho_{ge}(\tau)\Big\}, \quad (51)$$

$$\frac{\partial \rho_{gg}(t)}{\partial t} = 2\int_{t_0}^{t} d\tau |k(t-\tau)| \times\Big\{\cos[(t-\tau)\gamma - \phi(t-\tau)]\rho_{ee}(\tau) - \cos[(t-\tau)\gamma + \phi(t-\tau)]\rho_{gg}(\tau)\Big\}, \quad (52)$$

where the matrix elements are defines as $\rho_{ij}(t) = \langle i|\rho_S(t)|j\rangle$ with $|i,j\rangle$ being the ground state or the excited state of the qubit, and $\phi(t)$ is the phase of the reservoir correlation function $k(t) = |k(t)|e^{-i\phi(t)}$.

The qubit decoherence can be studied by the analysis of the spectral density $J(\epsilon_r, \epsilon_l)$. In the Literature, the density of states in the QPC reservoirs and the hopping amplitude across the QPC barrier are assumed to be energy-level independent, namely, the wide-band approximation for the QPC structure.[8, 10, 11, 12, 13, 14, 26] The spectral density is then given by

$$J(\epsilon_r, \epsilon_l) = \pi^2 g_L g_R |\Omega'|^2 . \quad (53)$$

This corresponds to the Markovian limit, in which the qubit dynamics is strongly decoherent[11, 12, 13, 14]. The Markovian dynamics arises from tunneling electrons in the QPC with a shortest time correlation $k(t-\tau) \propto \delta(t-\tau)$.

However, as indicated in Eqs. (48,49), the QPC structure determines the correlation time scale of the tunneling electron fluctuation in the QPC. The non-Markovian processes of the qubit dynamics emerges only when the QPC structure is casted with a finite correlation time scale. The effect of the QPC structure can be characterized by an energy-level dependence of the spectral density. In the literature, the spectral density $J_{RD}(\epsilon)$ for a reservoir coupling to a dot (or a molecular wire) is parameterized by Lorentzian spectrums,[17]

$$J_{RD}(\epsilon) = \frac{\pi}{2}\sum_{k=1}^{m} \frac{p_k \alpha_k}{(\epsilon - w_k)^2 + \alpha_k^2/4}, \quad (54)$$

where p_k, w_k and α_k are fitting parameters. The Lorentzian spectrum has also been applied to study

the quantum measurement of this system (using a constant hopping amplitude with a Lorentzian density of state).[29] For our system which involves electrons tunneling a barrier between two reservoirs, the spectral density can be approximately treated as

$$J(\epsilon_r,\epsilon_l)=\frac{\pi}{2}\frac{p\alpha}{(|\epsilon_r-\epsilon_l|-w)^2+\alpha^2/4}. \qquad (55)$$

In Eq. (55), the parameter p specifies the magnitude of the spectral density, w characterizes the variation of the barrier potential due to the interaction with the qubit electron, and the width α indicates a modulation of the decay rate for the qubit decoherence. Changing the variables of the integration in Eq. (48) from (ϵ,ϵ') to $(\varepsilon'=\frac{\epsilon+\epsilon'}{2},\varepsilon=\frac{\epsilon'-\epsilon}{2})$ and integrating out ε', we then obtain the following reservoir correlation function,

$$k(s) = \int_{-\infty}^{\infty}\frac{d\varepsilon}{2\pi}e^{-is\varepsilon}\frac{p\alpha}{4(|\varepsilon|-w)^2+\alpha^2} \times\Big\{\tilde{g}(\varepsilon-V_d)+\tilde{g}(\varepsilon+V_d)\Big\}, \qquad (56)$$

where the function $\tilde{g}(x)=\frac{x}{1-e^{-\beta x}}$.

A close connection between the qubit decoherence and the tunneling-electron fluctuation is revealed in Eq. (56). According to the spectral density in Eq. (55), the randomness of tunneling electrons across the QPC barrier is expounded first. Obviously, taking the limit $\alpha\ll|\epsilon_l-\epsilon_r|$ to Eq. (55), $J(\epsilon_r,\epsilon_l)$ reduces to $\pi^2\delta(|\epsilon_l-\epsilon_r|-w)$, only two channels $\epsilon_l-\epsilon_r=\pm w$ involved. On the other hand, $\alpha\gg|\epsilon_l-\epsilon_r|$ leads to a channel-mixture regime, where all transitions $\epsilon_l\rightleftarrows\epsilon_r$ that electrons tunneling between the source and the drain are allowed with the weight determined by $J(\epsilon_r,\epsilon_l)$. The randomness of electron tunneling processes in the channel-mixture regime comes from electron scattering which are determined by the band structure associated with the geometry of the two metal gates in the QPC and modulated by the interaction with the qubit electron. The parameter α in Eq. (55) characterizes the deviation describing how transfer energies $|\epsilon_l-\epsilon_r|$ in all electron tunneling processes are close to w in the statistics of ensemble average. The qubit dynamics with different α and an extreme small $w(\ll\gamma)$ are simulated in Fig. 3 with (a) and (b) for the qubit dephasing and (c) the qubit relaxation. The result shows that the qubit decoherence is suppressed as tunneling electrons with a smaller deviation. Associated with the qubit decay rate, α can be used to judge the decoherent behavior of the qubit state.

Furthermore, the reservoir time correlation function in Eq. (56) describes the time correlation of tunneling-electron fluctuation in the variation due to the measurement. In Fig. 4, the reservoir time correlation function is plotted in the condition that the variation of the QPC barrier potential has the same energy scale as the qubit system. It can be found in Fig. 4 (a) that the amplitude $|k(s)|$ is a Lorentzian profile with periodic deep peaks at $t=\pi/2w,\ 3\pi/2w,\ \cdots$. The amplitude $|k(t)|$ describes

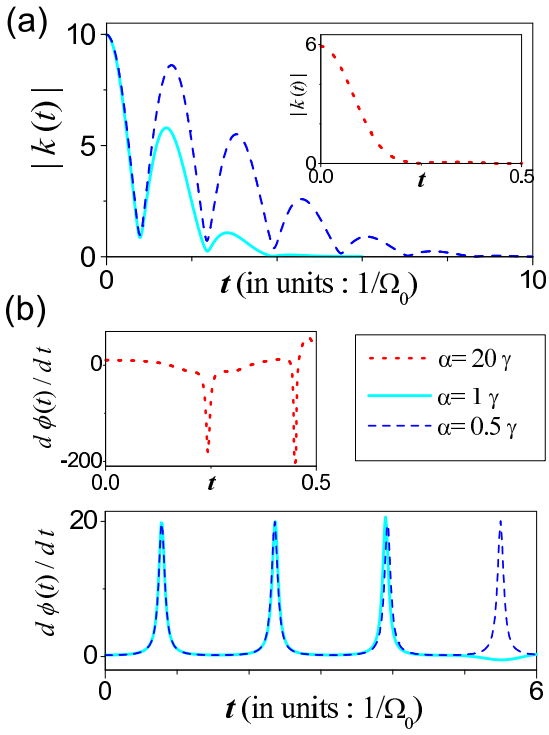

FIG. 4: (color online). The reservoir time correlation function plotted in the measurement condition that the variation of the QPC barrier potential has the same energy scale as the qubit system ($w=\gamma$) and with different α. The symmetric coupled quantum dots ($\gamma=2\Omega_0$) is considered. The following measurement parameters are used with Ω_0 being a rescaling factor: $\beta=1/\Omega_0$, $V_d=20\Omega_0$ and $p=\Omega_0$, respectively. (a) The amplitude of the reservoir time correlation function is plotted in units Ω_0^2. (b) The time derivative of the phase of the reservoir time correlation function is plotted in units Ω_0.

the correlation time scale between tunneling electrons which are induced by the measurement in the time interval t. With fixing the amplitude, the wider the half width of the Lorentzian profile of $|k(t)|$, the longer the time correlation of tunneling-electron fluctuation. Fig. 4 (a) then indicates that the time correlation increases with α decreasing. In other words, a shorter time correlation between electron tunneling processes leads to a more random electron-tunneling spectrum (with wide profile), see Eqs. (48,49). In the channel-mixture regime, the time correlation of tunneling-electron fluctuation is smeared, and the reservoir memory effect on the qubit dynamics is suppressed. The qubit dynamics with different α are simulated in Fig. 5. The result shows that in the channel-mixture regime ($\alpha=20\gamma$), the qubit undergoes a severe decoherence, which corresponds to the qubit dynamics in the Markovian limit. On the other hand, instructively, if the QPC structure can be recasted such that the measurement approaches to the case almost without random electron scatterings ($\alpha=0.5\gamma$), the non-Markovian processes of the qubit dynamics emerges. The qubit simply performs a periodic oscillation with small fluctuations. The qubit decoherence is suppressed. The mechanism of

the qubit decoherence can be understood by the analysis of the time derivative of the phase $\phi(t)$ in the reservoir time correlation function, which is plotted in Fig. 4 (b). According to Eq. (52), $d\phi(t)/dt$ characterizes the average transfer energy that the qubit electron obtains from all tunneling processes in the QPC. Fig. 4 (b) indicates that in the channel-mixture regime ($\alpha = 20\gamma$), the negative energy-transfer rate before $t = 0.25/\Omega_0$ leads to the qubit electron energy being exhausted. The contribution that the qubit electron absorbs energy from the QPC is very small and ignorable after $t = 0.25/\Omega_0$, because $|k(t)|$ decay to zero, see Fig. 4 (a). This effect occurs repeatedly due to the non-Markovian dynamical structure. The qubit finally relaxes to a mixed state, as shown in Fig. 5. However, for the case $\alpha = 0.5\gamma$, the qubit electron absorbs (emits) energy from (to) the QPC before (after) $t = \pi/2w, 3\pi/2w, \cdots$ in each period, as shown by the peaks with positive (negative) energy-transfer rates in Fig. 4 (b). The qubit is driven by the QPC periodically. Because of a longer time correlation of the tunneling-electron fluctuation [see the wide profile of $|k(t)|$ in Fig. 4 (a)], this periodic driving becomes significant. The qubit state is oscillating almost without decoherence, if the effect of the random electron scatterings can be ignored.

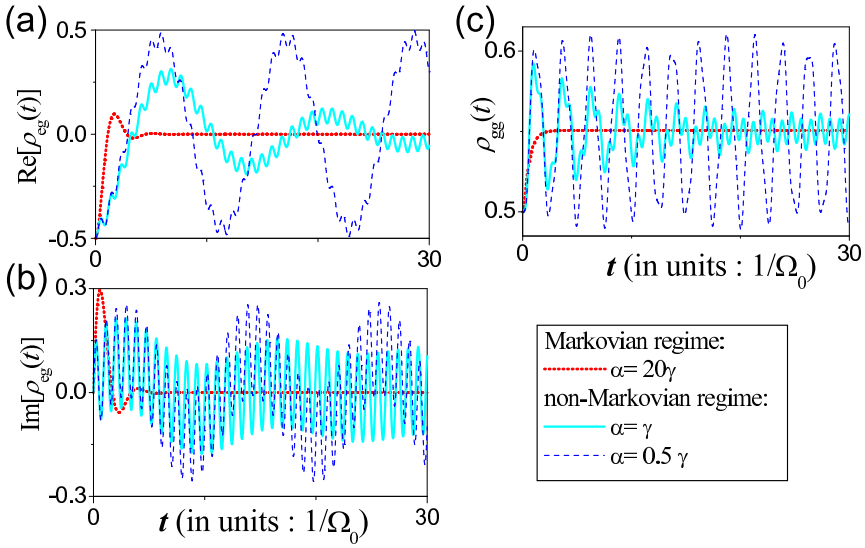

FIG. 5: (color online). The qubit dynamics measured in the condition $w = \gamma$ and with different α. The symmetric coupled quantum dots ($\gamma = 2\Omega_0$) is simulated. The qubit is set initially in the $|L\rangle$ state. The following measurement parameters are used with Ω_0 being a rescaling factor: $\beta = 1/\Omega_0$, $V_d = 20\Omega_0$ and $p = \Omega_0$, respectively. (a) and (b) for the qubit dephasing, and (c) the qubit relaxation.

Accordingly, the qubit decoherence also depends on the number of the peaks, which is determined by the variation of the barrier potential. By comparing Fig. 3 (d) and (e) with Fig. 4, it can be found that the number of the periodic peaks inside the half-width of the reservoir time correlation function indeed decreases with the parameter w decreasing. The more the sharp peaks with positive energy-transfer rates that the reservoir time correlation function contains, the larger amplitude of the oscillation the qubit performs in the asymptotic regime, specially, the population $\rho_{gg}(t)$ and the coherence $\mathrm{Re}[\rho_{eg}(t)]$. A large amount of energy transferred between the qubit electron and the tunneling electrons in the case with large w leads to a severer time variation (oscillation) on the qubit-electron population and the induced coherence. However, the w-dependence of the qubit dynamics is not so sensitive for the large α. The qubit decoherence under the QPC measurement with different w almost coincide, as indicated by the case of $\alpha = 20\gamma$ in Fig. 3 and Fig. 5. To drive the qubit state efficiently, tunneling electrons must be in the state with a longer time correlation, no matter how large the variation of the barrier is. Also, Fig. 3 (b) demonstrates that a sinusoidal quantum oscillation of the qubit coherence is still accessible under the quantum measurement, if the QPC structure is casted with a small w of the spectral density.

Finally, the numerical result also shows that the larger the bias voltage is applied, the shorter the time correlation of the tunneling-electron fluctuation becomes. A large amount of electrons tunneling across the QPC barrier forced by the large bias voltage leads to the time correlation of the tunneling-electron fluctuation being smeared with a sharp profile $|k(t)|$. Therefore, the qubit dynamics becomes typically Markovian, and the qubit

state is severely decoherent. The same decoherence behavior also occurs at a higher temperature. As a result, the constant spectral density used in literatures essentially describes electron tunneling processes with the most random channel mixture, and the qubit simply undergoes decoherent processes. More realistic non-Markovian dynamics emerges only when the effect of the explicit spectral density is taken into account. A particular design to cast the QPC structure such that tunneling electrons are in the state with longer time correlation could suppress the qubit decoherence during the QPC measurement.

V. SUMMARY

We have developed a non-equilibrium theory for the charge qubit dynamics accompanied with the QPC measurement. The effect of non-equilibrium fluctuation of the QPC reservoirs to the qubit dynamics has been treated by using the real-time diagrammatic technique developed based on Schwinger-Keldysh's approach. We introduce the loop operator to exactly derive the master equation for the reduced density operator, which is expressed in terms of the irreducible diagrams. The qubit decoherence is studied according to the resulted master equation up to the leading order. The non-Markovian processes in the qubit dynamics has been taken into account in this framework. We find that the qubit decoherence sensitively depends on the spectral density of the QPC structure. The constant spectral density in fact describes the electron tunneling processes with the most random channel mixture, which causes the severest qubit decoherence, and corresponds to the qubit dynamics in the Markovian limit. However, if the QPC structure can be controlled such that the spectral density with a narrower width, the electron tunneling processes reduce to a less channel mixture. The non-Markovian processes of the qubit dynamics emerges. The qubit simply performs a periodic oscillation with less decoherence. A longer time correlation of the tunneling-electron fluctuation results in the qubit state being periodically driven. In the channel-mixture regime, the time correlation of the tunneling-electron fluctuation is smeared by random electron scatterings. The qubit fails to be driven effectively by the QPC due to short time correlations of the tunneling-electron fluctuation, and the qubit state is simply decoherent. As the measurement operation is designed with the minimum deviation of electron tunneling processes, the qubit state could be measured with the least decoherence effect. The further work taking into account higher order contributions to the qubit decoherence and the noise spectrum of the QPC output signal is in progress.

Acknowledgments

The authors would like to thank S. A. Gurvitz for useful discussions. The work is supported by the National Center for Theoretical Science and National Cheng Kung University of Republic of China under Contract No. OUA 96-3-2-085, and National Science Council of Republic of China under Contract Nos. NSC-95-2112-M-006-001 and NSC-96-2112-M-006-011-MY3.

APPENDIX A: DERIVATION OF EQUATION OF MOTION IN EQUATION (7)

The equation of motion for the reduced density operator listed in Eq. (7) is derived in this appendix. In the interaction picture, the formal solution of the Liouville equation $\frac{\partial}{\partial t}\rho_{tot} = -i\,[H, \rho_{tot}]$ for the total density operator is given by

$$\hat{\rho}_{tot}(t) = \hat{\rho}_{tot}(t_0) - i\int_{t_0}^{t} d\tau[\hat{H}'_\tau, \hat{\rho}_{tot}(\tau)], \tag{A1}$$

iteratively, which leads to Dyson's perturbation expansion for the total density operator. However, to systematically build up the perturbation scheme for the kernel expansion in terms of the reservoir contour-order Green's functions (two-point correlation functions), alternatively, the second iteration of Eq. (A1)

$$\begin{aligned}\hat{\rho}_{tot}(t) = \hat{\rho}_{tot}(t_0) &- i\int_{t_0}^{t} d\tau[\hat{H}'_\tau, \hat{\rho}_{tot}(t_0)] \\ &- \int_{t_0}^{t} d\tau \int_{t_0}^{\tau} d\tau'[\hat{H}'_\tau, [\hat{H}'_{\tau'}, \hat{\rho}_{tot}(\tau')]],\end{aligned} \tag{A2}$$

which contains Hamiltonian operator orderings of $\hat{H}'_\tau$ and $\hat{H}'_{\tau'}$ in different time should be used. Obviously, as indicated by Eq. (A2), the total density operator obeys the following equation of motion

$$\frac{\partial}{\partial t}\hat{\rho}_{tot}(t) = -i\left[\hat{H}'_t, \hat{\rho}_{tot}(t_0)\right] - \int_{t_0}^{t} d\tau\left[\hat{H}'_t, \left[\hat{H}'_\tau, \hat{\rho}_{tot}(\tau)\right]\right]. \tag{A3}$$

Then, taking the partial trace to integrate out the degrees of freedom of the QPC reservoirs, Eq. (7) is resulted.

APPENDIX B: EXAMPLE OF CALCULATING THE COEFFICIENT $\mathcal{S}_{rl\cdots;i}$

In this appendix, we present an example of the contribution of the perturbation expansion Eq. (25) for $n = 2$ with the particular contour ordering $\{t \geq_p \tau \geq_p t_0 \geq_p (s_1, s_2)\}$ to illustrate how to diagrammatically calculate

the coefficient $\mathcal{E}_{rlr'l'r_1l_1r_2l_2}$ in Eq. (27),

$$\begin{aligned}
&\mathcal{S}_{rlr'l'r_1l_1r_2l_2}\Big(t\geq_p\tau\geq_p t_0\geq_p(s_1,s_2)\Big)\\
&\times\mathcal{E}_{rlr'l'r_1l_1r_2l_2}\Big(t\geq_p\tau\geq_p t_0\geq_p(s_1,s_2)\Big)\\
=\;&\hat{q}^+_{rl}(t)\hat{q}_{r'l'}(\tau)\rho_S(t_0)\tilde{T}\Big\{\hat{q}^+_{r_1l_1}(s_1)\hat{q}_{r_2l_2}(s_2)\Big\}\\
&\times\mathrm{Tr}_B\Big[\Big(\hat{\psi}^+_l(t)\hat{\psi}_r(t)\Big)\Big(\hat{\psi}^+_{r'}(\tau)\hat{\psi}_{l'}(\tau)\Big)\rho_B^{(0)}\\
&\times\tilde{T}\Big\{\Big(\hat{\psi}^+_{l_1}(s_1)\hat{\psi}_{r_1}(s_1)\Big)\Big(\hat{\psi}^+_{r_2}(s_2)\hat{\psi}_{l_2}(s_2)\Big)\Big\}\Big].
\end{aligned}\tag{B1}$$

The corresponding diagrams are shown in Fig. 6. It includes four topology-independent diagrams, two single-loop diagrams with the prefactor $(-1)^{(2+2)/2+1}=-1$ and two double-loop diagrams with the prefactor $(-1)^{(2+2)/2+2}=1$. The explicit expression of the coefficient $\mathcal{E}_{rlr'l'r_1l_1r_2l_2}$ of Eq. (B1) that the partial trace is carried out can be directly written down from four topology-independent diagrams

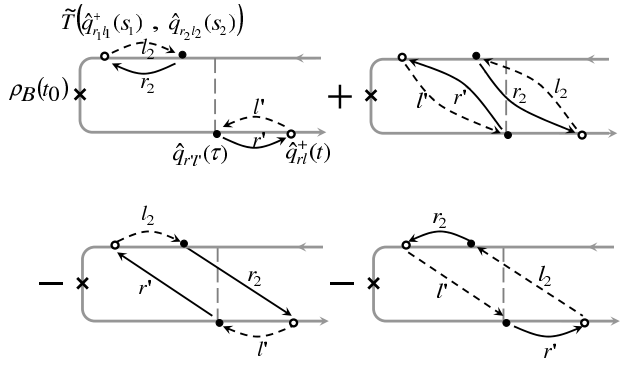

FIG. 6: Four topology-independent diagrams of the example Eq. (B1).

$$\begin{aligned}
&\mathcal{E}_{rlr'l'r_1l_1r_2l_2}\Big(t\geq_p\tau\geq_p t_0\geq_p(s_1,s_2)\Big)\\
=\;&\delta_{l_1l_2}\delta_{r_1r_2}\delta_{rr'}\delta_{ll'}G^{(0)}_{\tilde{F},l_2}(s_2,s_1)G^{(0)}_{\tilde{F},r_2}(s_1,s_2)\\
&\times G^{(0)}_{F,r'}(t,\tau)G^{(0)}_{F,l'}(\tau,t)\\
&+\delta_{l_1l'}\delta_{r_1r'}\delta_{l_2l}\delta_{r_2r}G^{(0)}_{<,l'}(\tau,s_1)G^{(0)}_{>,r'}(s_1,\tau)\\
&\times G^{(0)}_{>,l_2}(s_2,t)G^{(0)}_{<,r_2}(t,s_2)\\
&-\delta_{l_1l_2}\delta_{r_2r}\delta_{ll'}\delta_{r_1r'}G^{(0)}_{\tilde{F},l_2}(s_2,s_1)G^{(0)}_{<,r_2}(t,s_2)\\
&\times G^{(0)}_{F,l'}(\tau,t)G^{(0)}_{>,r'}(s_1,\tau)\\
&-\delta_{l_1l'}\delta_{rr'}\delta_{r_1r_2}\delta_{l_2l}G^{(0)}_{<,l'}(\tau,s_1)G^{(0)}_{F,r'}(t,\tau)\\
&\times G^{(0)}_{>,l_2}(s_2,t)G^{(0)}_{\tilde{F},r_2}(s_1,s_2).
\end{aligned}\tag{B2}$$

All coefficients $\mathcal{E}_{rlr'l'\ldots}$ for higher order contributions with arbitrary contour ordering can be calculated diagrammatically in the similar way.

APPENDIX C: THE LOOP OPERATORS FOR LEADING AND SECOND ORDER PERTURBATIONS

As an example, we illustrate how to write down the loop operators for the leading order kernel $K^{(0)}(t-\tau)*\rho_S(\tau)$ and the second order kernel $K^{(2)}(t-\tau)*\rho_S(\tau)$ diagrammatically. For the leading order kernel, only two topology-independent diagrams involves, and one is dual to the other. One of the both is shown in Fig. 7 (a).

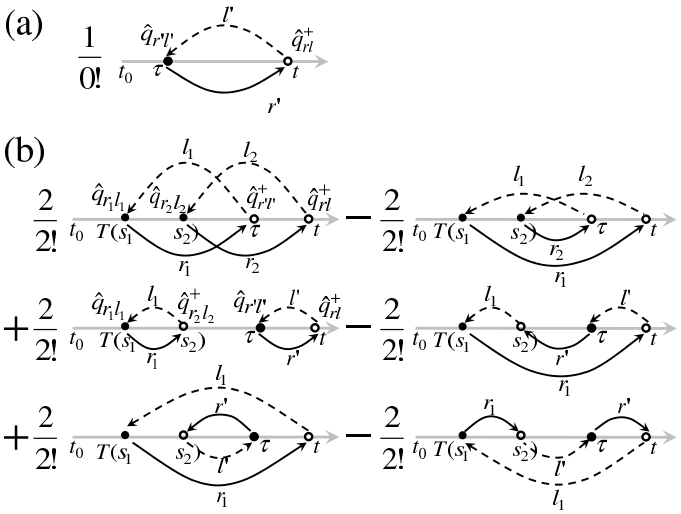

FIG. 7: Topology-independent diagrams of $K(t-\tau)*\rho_S(\tau)$ up to the second order perturbation. (a) and (b) The leading and the second order contributions

For the second order kernel with all possible time contour orderings, it contains totally 24 diagrams, half of them are dual to each other. We only need to consider one set of them (12 diagrams). Furthermore, one can find that only six topology-independent diagrams exist, see Fig. 7 (b). Each one corresponds to two topology-equivalent diagrams, i.e. the weight factor is 2 for each topology-independent diagram, while the prefactor is $\frac{-1}{2!}$ for the single-loop diagrams and $\frac{+1}{2!}$ for the double-loop diagrams.

The loop operators can be directly written down according to the topology-independent diagrams in Fig. 7. For the leading order kernel, the corresponding loop operator is given by $\frac{1}{0!}\hat{\mathcal{L}}_\tau\begin{pmatrix} t & \tau & t\\ & r' & l' & \end{pmatrix}$. We thus obtain the following expression

$$\begin{aligned}
&K^{(0)}(t-\tau)*\rho_S(\tau)\\
=\;&Q_S(t-t_0)\Big\{\hat{\mathcal{L}}_\tau\begin{pmatrix} t & \tau & t\\ & r' & l' & \end{pmatrix}\\
&\times\mathcal{J}(\hat{q},\hat{q}^+;\vec{\alpha},\vec{\gamma})\Big|_{\vec{\gamma}=\vec{\gamma}'=\{\vec{\alpha}\}=0}+\text{duality}\Big\}.
\end{aligned}\tag{C1}$$

Similarly, the explicit expression of the second order kernel can also be obtained according to the topology-

independent diagrams in Fig. 7 (b),

$$\begin{aligned} & K^{(2)}(t-\tau) * \rho_S(\tau) \\ = \; & Q_S(t-t_0)\Big\{\hat{\mathcal{K}}^{(2)}(t-\tau)\mathcal{J}(\hat{q},\hat{q}^+;\vec{\alpha},\vec{\gamma})\Big|_{\vec{\gamma}=\vec{\gamma}'=\{\vec{\alpha}\}=0} \\ & +\text{duality}\Big\}, \end{aligned} \tag{C2}$$

$$\begin{aligned} & \hat{\mathcal{K}}^{(2)}(t-\tau) \\ = \; & \frac{2}{2!}\hat{\mathcal{L}}_\tau \begin{pmatrix} \tau & & s_1 & & \tau \\ & r_1 & & l_1 & \end{pmatrix} \cdot \hat{\mathcal{L}}_\tau \begin{pmatrix} t & & s_2 & & t \\ & r_2 & & l_2 & \end{pmatrix} \\ & -\frac{2}{2!}\hat{\mathcal{L}}_\tau \begin{pmatrix} t & & s_1 & & \tau & & s_2 & & t \\ & r_1 & & l_1 & & r_2 & & l_2 & \end{pmatrix} \\ & +\frac{2}{2!}\hat{\mathcal{L}}_\tau \begin{pmatrix} s_2 & & s_1 & & s_2 \\ & r_1 & & l_1 & \end{pmatrix} \cdot \hat{\mathcal{L}}_\tau \begin{pmatrix} t & & \tau & & t \\ & r' & & l' & \end{pmatrix} \\ & -\frac{2}{2!}\hat{\mathcal{L}}_\tau \begin{pmatrix} t & & s_1 & & s_2 & & \tau & & t \\ & r_1 & & l_1 & & r' & & l' & \end{pmatrix} \\ & +\frac{2}{2!}\hat{\mathcal{L}}_\tau \begin{pmatrix} \tau & & s_2 & & \tau \\ & l' & & r' & \end{pmatrix} \cdot \hat{\mathcal{L}}_\tau \begin{pmatrix} t & & s_1 & & t \\ & r_1 & & l_1 & \end{pmatrix} \\ & -\frac{2}{2!}\hat{\mathcal{L}}_\tau \begin{pmatrix} t & & \tau & & s_2 & & s_1 & & t \\ & r' & & l' & & r_1 & & l_1 & \end{pmatrix}. \end{aligned} \tag{C3}$$

Note that all contour-ordering $\{T_{\tilde{p}_i}\}$ of the leading and the second order perturbations have been taken into account in Eqs. (C1,C3) combining with their duality, respectively.

In addition, we can express each order of the kernel in terms of the loop operators associated with the irreducible diagrams, for instance,

$$\begin{aligned} & K^{(0)}(t-\tau) * \rho_S(\tau) \\ = \; & Q_S(t-t_0)\hat{\mathcal{L}}_{ir,\tau}\left(t,\tau,t\right)\mathcal{J}(\hat{q},\hat{q}^+;\vec{\alpha},\vec{\gamma})\Big|_{\vec{\gamma}=\vec{\gamma}'=\{\vec{\alpha}\}=0}, \end{aligned}$$

$$\begin{aligned} & K^{(2)}(t-\tau) * \rho_S(\tau) \\ = \; & Q_S(t-t_0)\Big\{\hat{\mathcal{L}}_{in,\tau}\left[s_1,s_2,s_1\right]\cdot\hat{\mathcal{L}}_{ir,\tau}\left(t,\tau,t\right) \\ & +\hat{\mathcal{L}}_{ir,\tau}\left(\tau,s_2,\tau\right)\cdot\hat{\mathcal{L}}_{ir,\tau}\left(t,s_1,t\right)-\hat{\mathcal{L}}_{ir,\tau}\left(t,s_1,s_2,\tau,t\right) \\ & -\hat{\mathcal{L}}_{ir,\tau}\left(t,s_1,\tau,s_2,t\right)-\hat{\mathcal{L}}_{ir,\tau}\left(t,\tau,s_1,s_2,t\right)\Big\} \\ & \times\mathcal{J}(\hat{q},\hat{q}^+;\vec{\alpha},\vec{\gamma})\Big|_{\vec{\gamma}=\vec{\gamma}'=\{\vec{\alpha}\}=0}. \end{aligned} \tag{C4}$$

Therefore, we can resum all perturbation orders of $K(t-\tau)*\rho_S(\tau)$ according to the irreducible diagrams.

[1] E. Buks, R. Schuster, M. Heiblum, D. Mahalu and V. Umansky, Nature **391**, 871 (1998); T. Hayashi, T. Fujisawa, H. D. Cheong, Y. H. Jeong, and Y. Hirayama, Phys. Rev. Lett. **91**, 226804 (2003); J. M. Elzerman, R. Hanson, L. H. Willems van Beveren, B. Witkamp, L. M. K. Vandersypen and L. P. Kouwenhoven, Nature **430**, 431 (2004); J. R. Petta, A. C. Johnson, J. M. Taylor, E. A. Laird, A. Yacoby, M. D. Lukin, C. M. Marcus, M. P. Hanson, and A. C. Gossard, Science **309**, 2180 (2005); F. H. L. Koppens, C. Buizert, K. J. Tielrooij, I. T. Vink, K. C. Nowack, T. Meunier, L. P. Kouwenhoven, and L. M. K. Vandersypen, Nature **442**, 766 (2006).

[2] R. G. Knobel and A. N. Cleland, Nature **424**, 291 (2003).

[3] Y. Makhlin, G. Schön and A. Shnirman, Rev. Mod. Phys. **73**, 357 (2001).

[4] I. Chiorescu, Y. Nakamura, C. J. P. M. Harmans, J. E. Mooij, Science **299**, 1869 (2003); N. Katz, M. Ansmann, R. C. Bialczak, E. Lucero, R. McDermott, M. Neeley, M. Steffen, E. M. Weig, A. N. Cleland, J. M. Martinis, and A. N. Korotkov, Science **312**, 1498 (2006); A. Lupascu, S. Saito, T. Picot, P. C. De Groot, C. J. P. M. Harmans and J. E. Mooij, Nature Phys. **3**, 119 (2007).

[5] D. Loss and D. P. DiVincenzo, Phys. Rev. A **57**, 120 (1998); B. E. Kane, Nature **393**, 133 (1998); W.-M. Zhang, Y.-Z. Wu, C. Soo, and M. Feng, Phys. Rev. B **76**, 165311 (2007).

[6] V. B. Braginsky and F.Ya. Khalili, *Quantum Measurement* (Cambridge University Press, Cambridge, England, 1992); M. Namiki, S. Pascazio, and H. Nakazato, *Decoherence and Quantum Measurements* (World Scientific, Sigapore, 1997).

[7] B. J. van Wees, H. van Houten, C. W. J. Beenakker, and J. G. Williamson., Phys. Rev. Lett. **60**, 848 (1988); M. Field, C. G. Smith, M. Pepper, D. A. Ritchie, J. E. F. Frost, G. A. C. Jones, and D. G. Hasko, Phys. Rev. Lett. **70**, 1311 (1993).

[8] S. A. Gurvitz, Phys. Rev. B **56**, 15215 (1997); S. A. Gurvitz, quant-ph/9808058.

[9] Y. M. Blanter and M. Buttiker, Phys. Rep. **336**, 1 (2000); S. Pilgram and M. Buttiker, Phys. Rev. Lett. **89**, 200401 (2002); A. A. Clerk, S. M. Girvin, and A. D. Stone, Phys. Rev. B **67**, 165324 (2003); D. V. Averin and E. V. Sukhorukov, Phys. Rev. Lett. **95**, 126803 (2005).

[10] A. N. Korotkov, Phys. Rev. B **60**, 5737 (1999); A. N. Korotkov and D. V. Averin, Phys. Rev. B **64**, 165310 (2001).

[11] H.-S. Goan, G. J. Milburm, H. M. Wiseman, and H. B. Sun, Phys. Rev. B **63**, 125326 (2001).

[12] T. M. Stace and S. D. Barrett, Phys. Rev. Lett. **92**, 136802 (2004).

[13] X. Q. Li, P. Cui, nd Y. J. Yan, Phys. Rev. Lett. **94**, 066803 (2005).

[14] M.-T. Lee and W.-M. Zhang, Phys. Rev. B **74**, 085325 (2006).

[15] W. A. Coish and D. Loss, Phys. Rev. B **70**, 195340 (2004).

[16] A. Braggio, J. König, and R. Fazio, Phys. Rev. Lett. **96**, 026805 (2006).

[17] S. Welack, M. Schreiber, and U. Kleinekathofer, J. Chem. Phys. **124**, 044712 (2006).

[18] J. Schwinger, J. Math. Phys. **2**, 407 (1961); L. V. Keldysh, Zh. Eksp. Thor. Fiz. **47**, 1515 [Sov. Phys.-JETP

20, 1018 (1965)].
[19] J. Rammer and H. Smith, Rev. Mod. Phys. **58**, 323 (1986); H. Haug and A.-P. Jauho, *Quantum Kinetics in Transport and Optics of Semiconductors* (Springer, Berlin, 1996).
[20] K.-C. Chou, Z.-B. Su, B.-L. Hao and L. Yu, Phys. Rep. **118**, 1 (1985); W.-M. Zhang and L. Wilets, Phys. Rev. C **45**, 1900 (1992).
[21] H. Schoeller and G. Schön, Phys. Rev. B **50**, 18436 (1994).
[22] M. Kindermann and Y. V. Nazarov, Phys. Rev. Lett. **91**, 136802 (2003); Y. Utsumi, D. S. Golubev and G. Schön, Phys. Rev. Lett. **96**, 086803 (2006).
[23] A. Rosch, J. Kroha and P. Wölfle, Phys. Rev. Lett. **87**, 156802 (2001).
[24] H. Schoeller and J. König, Phys. Rev. Lett. **84**, 3686 (2000).
[25] J. G. König, H. Schoeller, and G. Schön, Phys. Rev. Lett. **76**, 1715 (1996).
[26] A. Shnirman, D. Mozyrsky and I. Martin, cond-mat/0211618.
[27] R. W. Zwanzig, *Lectures in Theorectical Physics* (Wiley, New York, 1961); H. Mori, Prog. Theor. Phys. **33**, 423 (1965); Y. J. Yan, Phys. Rev. A **58**, 2721 (1998).
[28] X. Q. Li and Y. J. Yan, Phys. Rev. B **75**, 075114 (2007).
[29] B. Elattari and S. A. Gurvitz, Phys. Rev. A, **62**, 032102 (2000).